Journal Name

Dynamic Article Links ►

Cite this: DOI: 10.1039/c0xx00000x

www.rsc.org/xxxxxx

ARTICLE TYPE

Kinetics of light-driven oxygen evolution at α-Fe_2O_3 electrodes

Laurence M. Peter[a,*], K.G. Upul Wijayantha[b], Asif A. Tahir[b]

Received (in XXX, XXX) Xth XXXXXXXXX 20XX, Accepted Xth XXXXXXXXX 20XX
DOI: 10.1039/b000000x

The kinetics of light-driven oxygen evolution at polycrystalline α-Fe_2O_3 layers prepared by aerosol-assisted chemical vapour deposition has been studied using intensity modulated photocurrent spectroscopy (IMPS). Analysis of the frequency-dependent IMPS response gives information about the competition between the 4-electron oxidation of water by photogenerated holes and losses due to electron-hole recombination via surface states. The very slow kinetics of oxygen evolution indicates the presence of a kinetic bottleneck in the overall process. Surface treatment of the α-Fe_2O_3 with dilute cobalt nitrate solution leads to a remarkable improvement in the photocurrent response, but contrary to expectation, the results of this study show that this is not due to catalysis of hole transfer but is instead the consequence of almost complete suppression of surface recombination.

Introduction

Low-cost efficient water splitting using sunlight remains one of the major scientific challenges for photoelectrochemistry. The energetic criteria for light-driven water splitting arise from the need to match the free energy of electrons and holes to the proton and oxygen reduction potentials respectively. In addition, the semiconductor electrode needs to be stable under illumination. In practice, oxide semiconductors are more stable, than for example, chalcogenides such as CdS or III-V compounds like GaAs However, only wide band gap semiconductors (e,g.$SrTiO_3$: band gap E_g = 3.2 eV) satisfy the energetic criteria for photoelectrochemical water splitting without external voltage bias. However the wide band gap of such oxides limits light absorption to the ultraviolet part of the solar spectrum, so such materials are not suitable for high efficiency water splitting. Other oxide materials such as α-Fe_2O_3 (E_g = 2.0 eV) have the advantage that they absorb visible light, but in general their electronic affinities are too high, so their conduction band energies lie below the hydrogen potential. By contrast, the energy match for water oxidation by photogenerated holes is favourable, with the valence bands of many oxides lying well below the oxygen potential. Although the search for stable oxides with lower electron affinities continues[1], application of currently available oxides such as α-Fe_2O_3 for water splitting requires application of an external voltage bias. This can be achieved in a tandem cell configuration[2] in which light transmitted through the oxide is absorbed by a solar cell that provides the additional voltage required to bias the metal cathode so that hydrogen generation can take place. However, the efficiencies of such cells[3] is currently much lower than the 15% predicted for an ideal tandem configuration based on α Fe_2O_3.[4] In the case of tandem cells employing α-Fe_2O_3 as the photoanode, the main problem is the poor optoelectronic properties of the oxide[2]. The transport of electrons and holes in α-Fe_2O_3 is strongly anisotropic and appears to occur via small polaron hopping involving Fe(II)-Fe(II) and Fe(III)-Fe(IV) pairs respectively.[5] The low mobility and short lifetime of holes in the bulk lead to a short hole diffusion length, so that collection of holes is almost entirely restricted to the space charge region created at the oxide electrolyte interface. Typically, the optical penetration depth for visible wavelengths into α-Fe_2O_3 is more than an order of magnitude greater than the width of the space charge region, so that a large fraction of the photogenerated electron hole pairs recombine in the bulk of the material. These problems have been addressed by nanostructuring the α-Fe_2O_3 to increase the chances of holes reaching the oxide/electrolyte interface.[6-8] However, even in the case where holes manage to reach the oxide/electrolyte interface, the 4-electron oxidation of water has to compete with surface recombination of electrons and holes. The present paper describes a study of this competition carried out using intensity modulated photocurrent spectroscopy (IMPS).[9, 10] This technique, which involves measuring the frequency response of the photocurrent to sinusoidal modulation of the illumination intensity, provides information about the rate constants for electron transfer and recombination. The method, which has been used in our earlier work to study photoelectrochemical reactions at passive iron electrodes.[11], is related to electrochemical impedance spectroscopy (PEIS)[12, 13], in which the light intensity is held constant and the electrode potential is modulated. We have recently reported a PEIS study of oxygen evolution at illuminated α-Fe_2O_3 [14].

The mechanism of 4-electron oxidation of water at α-Fe_2O_3 is not known. However, it is reasonable to suppose that the process involves the formation of higher-valent Fe states at surface sites. Fe(IV)[15] and Fe(VI)[16] states are known to be formed by electrochemical oxidation of iron or iron oxide, and both Fe(VI) and Fe(V) has also been studied as an environmentally friendly oxidants.[17] The 4-electron oxidation of water could involve successive hole capture to reach oxidation states up to Fe(VI), which is metastablele in alkaline solution as ferrate(VI) ion,

FeO_4^{2-}, which decomposes slowly to produce oxygen and FeOOH.[18]

The formation of Fe(V) species on the surface would involve the sequential capture of two holes. However, 4 holes are needed to oxidise 4 OH^- ions to dioxygen and water in alkaline solution. For this reason, the mechanism could involve a bimolecular step. In a previous paper, we suggested as an example the following sequence.

$$Fe(III) + h^+ \rightarrow Fe(IV)$$
$$Fe(IV) + h^+ \rightarrow Fe(V)$$
$$2\,Fe(V) + 4\,OH^- \rightarrow 2\,Fe(III) + 2H_2O + O_2$$

Scheme I

Here the final step would involve OH ligands bound to adjacent Fe(V) sites. This bimolecular step could be responsible for a 'kinetic bottleneck' in the oxygen evolution reaction. In an alternative reaction scheme, Fe(VI) could be formed by the successive capture of three holes at a surface Fe(III) site, and oxygen would then evolved in step such as

$$Fe(VI) + 4OH^- + h^+ \rightarrow Fe(III) + 2H_2O + O_2$$

Scheme II

A possible clue to the chemical identity of the surface intermediate is given by the results of a recent study of water oxidation on α-Fe_2O_3 utilizing transient absorption spectroscopy[19] which show a photo-induced absorption peak at 580nm, which could be due to Fe(VI) states at or near the surface (the absorption spectrum of the FeO_4^{2-} ion in alkaline solution exhibits a broad peak at 500 nm.[20, 21])

Mechanisms of the kind shown in Schemes I and II share the common feature that they involve the 'storing' of holes at the surface that is necessary to allow oxygen evolution to take place. The stored holes can be thought of as 'surface trapped holes' located on surface states. These states should also be able to capture electrons as well as holes, and in this case the process is equivalent to surface recombination. Scheme I, for example, needs to be modified to take this into account as shown in Scheme III.

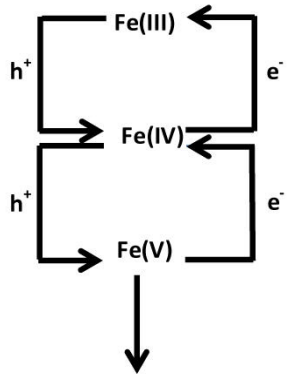

Scheme III

Here the hole capture processes on the left compete with the recombination pathways on the right. It is important to note here that these recombination pathways may not be the only routes for electron-hole recombination at the surface. Surface recombination via surface states (due, for example, to defects) commonly occurs at semiconductor electrodes even when a one electron redox system is present.

The quantum efficiency of the photoelectrochemical oxygen evolution reaction depends on the product of two factors: η_{coll}, the fraction of holes collected by drift/diffusion and η_{trans}, the fraction of those holes transferred successfully at the interface to produce oxygen. Nanostructuring of the oxide layer[22] optimizes η_{coll},, and surface modification by catalysts should in principle enhance η_{trans}. A recent report[23] suggests that a photodeposited form of the cobalt oxide catalyst developed by Kanan and Nocera[24] catalyzes photoelectrochemical oxygen evolution on α-Fe_2O_3, and Kay et al.[25] have attributed a similar improvement in performance of α-Fe_2O_3 electrodes achieved by treatment with an aqueous Co(II) solution to formation of catalytic sites on the surface. By contrast, the substantial improvement in photocurrent response of α-Fe_2O_3 achieved recently using deposition of ultrathin Al_2O_3 layers by ALD has been attributed to passivation of surface states.[26] The present paper deals with the determination of η_{coll} and η_{trans} using IMPS and the effects of treating the electrode surface with a dilute cobalt nitrate solution, which has been reported to enhance the performance of α-Fe_2O_3 electrodes for water splitting.[25] Details of the determination of η_{coll} and η_{trans} by PEIS can be found elsewhere.[14]

Theory

The theory of IMPS has been developed previously for simple 1-electron transfer reactions as well as for more complex reactions involving multiple steps.[9, 10, 12, 13, 27] A generalized phenomenological theory developed in our earlier work[10] was used to describe the system in the present study since the mechanism of oxygen evolution at α-Fe_2O_3 is unknown. In general, the phenomenological description can be reconciled with particular mechanisms[28], but this will not be attempted here. The theory considers competition between hole capture and surface recombination as shown in Figure 1.

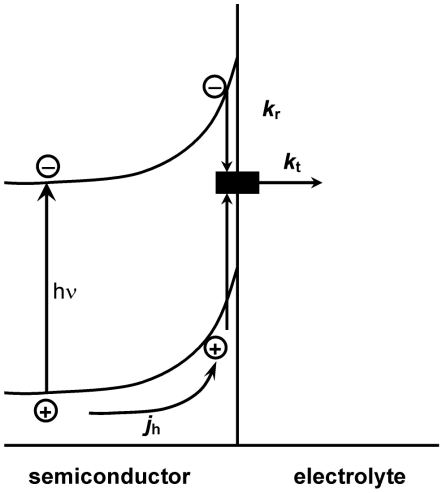

Fig 1. Generalized reaction scheme showing competition between charge transfer and recombination. j_h is the hole flux into the surface and k_t and k_r are first order rate constants for charge transfer and surface recombination respectively.

Here k_t and k_r are first order rate constants. The rate of interfacial charge transfer is given by the product of k_t and the surface hole concentration, p_{surf}. The rate of surface recombination is given by the product $k_r p_{surf}$. k_r is a pseudo first order rate constant that depends on the surface electron concentration: $k_r = k_r'[n_{surf}]$, where k_r' is given by the product of the thermal velocity of electrons v_{th} and the electron capture cross section σ_n of the surface states.

The time-dependent photocurrent response of a semiconductor electrode to a square illumination pulse can be understood on the basis of the model in Fig. 1 as follows. When the electrode is illuminated, an almost instantaneous hole current (j_h) flows into the surface. In the absence of recombination in the space charge region, j_h is given by the Gärtner equation[29]

$$j_h = qI_0\left(1-\frac{e^{-\alpha W}}{1+\alpha L_p}\right) \quad (1)$$

where I_0 is the incident photon flux corrected for reflection loss, α is the absorption coefficient of the oxide, W is the width of the space charge region and L_p is the hole diffusion length. In the case of α-Fe_2O_3, $\alpha L_p << 1$, so that the hole current is determined by αW, which is typically of the order of 0.1 or less. This means that the collection efficiency, $\eta_{coll} = j_h / qI_0$ will be rather low. Eq. 1 applies only to smooth electrodes where the directions for light absorption and hole transport are the same. The objective of nanostructuring α-Fe_2O_3electrodes is to enable more efficient three dimensional collection of holes by nearby surfaces. The capture of holes by surface states leads to a build-up of trapped holes, and as a consequence an electron current is induced as electrons recombine with the trapped holes. The photocurrent measured in the external circuit therefore falls from its initial value as the electron current increases towards its steady state value. Now when the illumination is interrupted, the hole current ceases virtually instantaneously, and the remaining holes trapped in the surface recombine with electrons, giving a current of opposite sign to that observed during the illumination phase. These processes give rise to the characteristic decay and overshot of the photocurrent as shown in Fig 2.

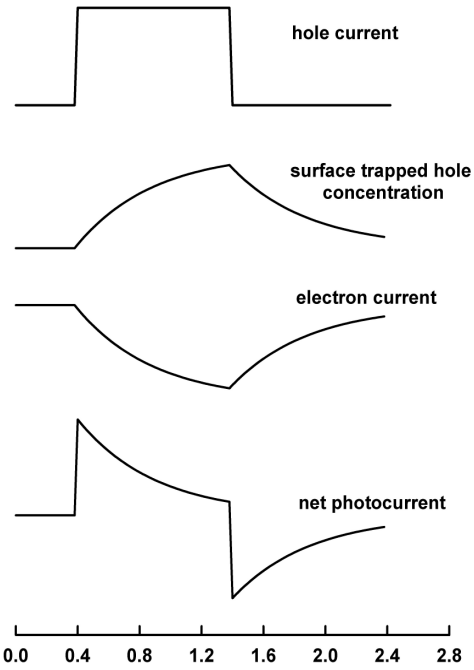

Fig 2. Origin of the characteristic shape of the photocurrent response to square wave illumination.

The time constant associated with the decay of the photocurrent is given by $k_r + k_t$, and the ratio of the steady state photocurrent to the instantaneous photocurrent observed when the illumination is switched on is given by the ratio $k_t / (k_r + k_t)$.

The photocurrent response to intensity modulated illumination can be understood using the same scheme. It can be seen from Fig. 2 that the electron current lags behind the hole current, but has the opposite sign, so that for a particular modulation frequency, the IMPS response can be determined from the vector diagram shown in Fig. 3

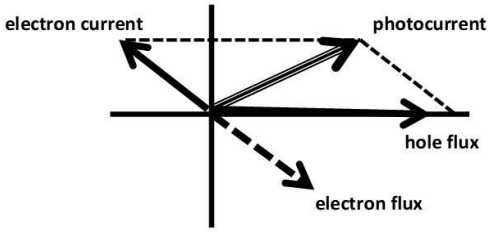

Fig 3. Vector diagram for IMPS showing the phase relationships between the hole and electron currents and the resulting photocurrent.

It can be shown that the IMPS response as a function of frequency is given by eq. 2, which corresponds to a semicircle in the complex plane as shown in normalized form in Fig. 4.

$$\frac{j_{photo}}{j_h} = \frac{k_t + i\omega}{k_t + k_r + i\omega} \quad (2)$$

The high frequency intercept should occur at unity since the measured current is equal to the hole current (i.e. no

recombination). The normalized low frequency intercept corresponds to the fraction of the hole flux that undergoes interfacial electron transfer, $k_t/(k_r+ k_t)$]. The radial frequency at the maximum of the semicircle is given by the sum $k_t + k_r$.

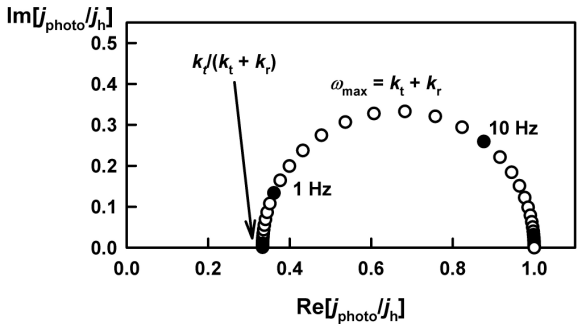

Fig.4. IMPS response corresponding to the kinetic scheme in Fig. 1. $k_t = 10\ s^{-1}$, $k_r = 20\ s^{-1}$.

In practice, the high frequency part of the IMPS response is attenuated by the RC time constant of the electrochemical cell. In the case of the α-Fe_2O_3 films studied here, the RC time constant arises from the series resistance of the fluorine-doped tin oxide (FTO) glass used as substrate and the (high) space charge capacitance of the oxide film. The effect of RC attenuation is illustrated by the calculated response shown in Fig. 5. RC attenuation clearly complicates the analysis of the IMPS response, but provided that the RC time constant is at least two decades smaller than $1/(k_t + k_r)$, the errors in using the analysis shown in Fig. 4 are acceptably small.

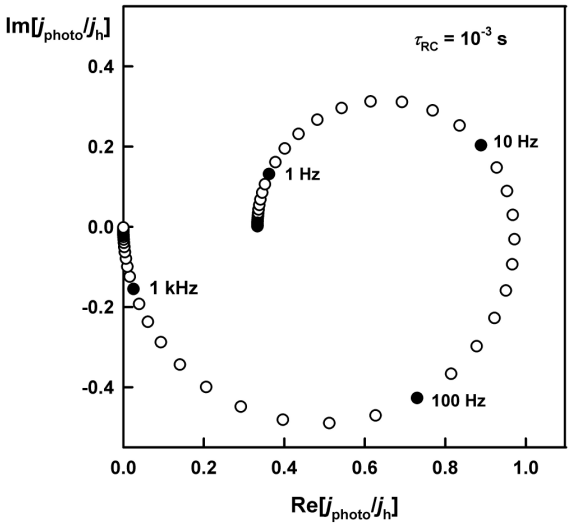

Fig 5. RC attenuation of high frequency part of the IMPS response. k_t and k_r values as in Fig. 4. RC time constant 10^{-3}s.

Interpretation of the first order rate constants k_t and k_r in terms of a proposed reaction mechanism involves consideration of the steady state expressions for the concentrations of surface intermediates and definition of a rate determining step.[28] In view of the complexity of the expressions for multiple electron transfer reaction schemes, this approach is not developed in this paper.

Experimental

Preparation of α-Fe_2O_3 films

Smooth polycrystalline α-Fe_2O_3 films were deposited by aerosol-assisted chemical vapour deposition (AACVD) on FTO-coated glass substrates (1cm x 2cm pieces of Pilkington TEC 8, 8 Ω/square) using a reactor tube located in a tube furnace. Further details of the AACVD assembly can be found elsewhere.[30] Part of one end of the FTO substrate was masked by a microscope slide to prevent Fe_2O_3 deposition so that electrical contacts could be made for the electrochemical and photoelectrochemical measurements. Substrates were cleaned ultrasonically with distilled water, acetone, isopropanol and ethanol before being placed in the reactor tube and heated to 450 ºC for 20 min before starting the deposition. The aerosol was generated from a 0.05 M solution of ferrocene (98%, Lancaster Synthesis) in toluene by positioning a round bottomed flask with the precursor solution in a water bath above the piezoelectric modulator of an ultrasonic humidifier. The aerosol droplets were transported to the heated substrate by the air flow. The flow rate (150 ml/min) was controlled by a thermal mass flow controller (Bronkhorst UK Ltd.). The deposition time was 45 minutes. SEM micrographs of the films can be found in an earlier paper.[14]

IMPS and photoresponse measurements

IMPS measurements on the α-Fe_2O_3 electrodes were conducted using a potentiostat in a three-electrode configuration with a Ag|AgCl,KCl reference electrode, and a platinum wire counter electrode. The electrolyte was 1 M NaOH. Some electrodes were treated by placing a drop of 10 mM cobalt nitrate solution[25] on the surface for 1 minute before rinsing thoroughly with de-ionized water. Modulated illumination was provided by a high intensity light-emitting diode (LED: 455 nm) controlled by a home-built LED driver that allowed superimposition of sinusoidal modulation (typically less than 10%) on a dc illumination level. The sine wave signal was provided by a Solartron 1250 frequency response analyzer. The intensity of the illumination was varied using calibrated neutral density filters and measured using a calibrated silicon photodiode. The frequency response of the potentiostat as function of current sensitivity was measured using a dummy cell, and data collection was limited to the frequency range where phase shifts arising from the potentiostat could be neglected. Incident photon to electron conversion efficiency (IPCE) spectra were measured in the conventional way.

Results and Discussion

The effects of surface recombination are illustrated by the photocurrent transients shown in Fig. 6, which resemble the net photocurrent plot in Fig 2. The relaxation time constants are remarkably long, showing that the rate constants k_t and k_r are of the order of 1 s^{-1}. This is consistent with a slow rate determining step causing 'kinetic bottleneck' in the oxygen evolution mechanism as well as with slow recombination. If higher-valent Fe states are formed as intermediates as suggested in Scheme III, their electron capture cross sections must be remarkably small. This may indicate that they may carry a negative charge, possibly as a consequence of binding hydroxide ions. Interestingly, the

slow decay of the photocurrent seen in Fig. 6 closely resembles the decay in transient absorption at 580 nm reported by Pendlebury et al[19]., who attributed it to surface trapped holes.

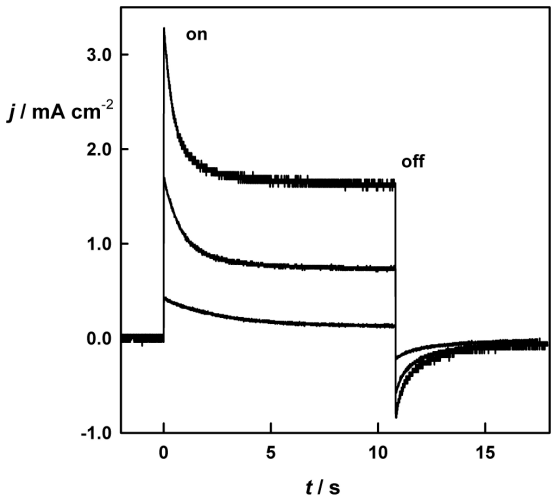

Fig 6. Photocurrent transients measured at 0 V vs. Ag|AgCl. Illumination 455 nm. Photon flux (top to bottom): 1.1 x 10^{17} cm^2 s^{-1}; 4.0 x 10^{16} cm^{-2} s^{-1}; 1.33 x 10^{16} cm^2 s^{-1}.

The IMPS response of the α-Fe_2O_3electrodes was typically measured over the potential range -0.7 V to 0.6 V vs. Ag|AgCl at 100 mV intervals and at different light intensities. A modulation depth of ca. 10% was used to ensure linear response. An example of an experimental IMPS plot in the complex plane is shown in Fig. 7.

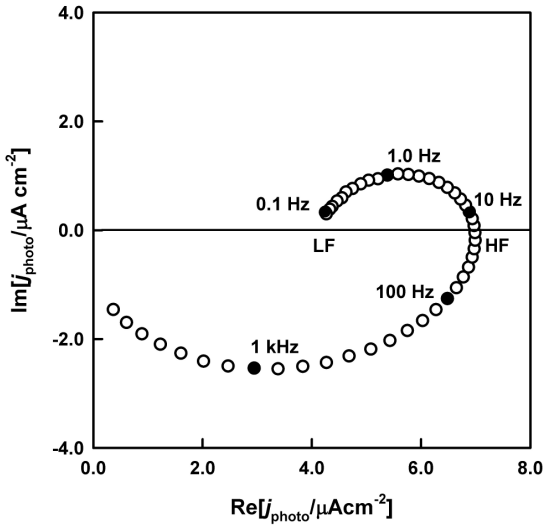

Fig. 7. Typical IMPS response showing semicircle in upper quadrant due to the competition between charge transfer and recombination and - in the lower quadrant - attenuation due to the RC time constant of the electrode. Cobalt- treated α-Fe_2O_3 sample, -0.3 V vs. Ag|AgCl. Illumination 455 nm, dc photon flux 1.1 x 10^{17} cm^2 s^{-1}

It can be seen from Fig. 7 that the frequencies of the upper and lower 'semicircles' differ at least 2 decades, so that reasonable reliable kinetic data can be extracted using the analysis shown in Fig. 4. The low frequency intercept (LF in Fig. 7) and the high frequency crossing point (HF in Fig. 7) were used together with the radial frequency of the maximum to derive the values of k_t and k_r.

It can be seen from Fig. 7 that the response in the lower quadrant due to RC attenuation is flattened considerably, and this can probably be attributed in part to the fact that the dielectric constant of α-Fe_2O_3 is frequency dependent[31], although surface inhomogeneity may also play a role. This frequency dependence can also be inferred from Fig. 8, which shows the capacitance derived from the electrode admittance measured in the dark as a function of frequency.

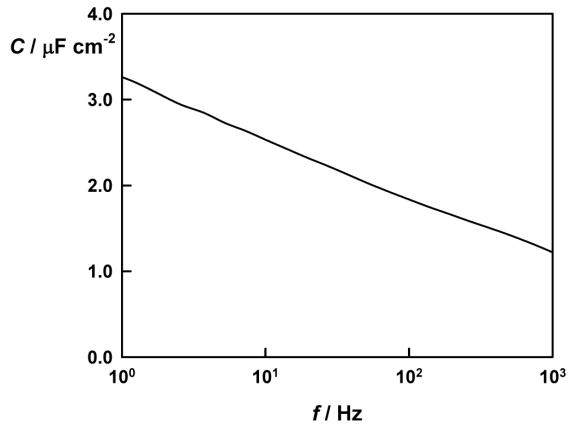

Fig. 8. Frequency dependent capacitance of α-Fe_2O_3 electrode measured at 0.0 V vs. Ag|AgCl in the dark.

For this reason analysis of the IMPS response was confined to the upper quadrant, where the effects of RC attenuation can be neglected. The frequency dispersion of the capacitance also complicates reliable determination of the doping density of α-Fe_2O_3 films by capacitance voltage measurements.

As shown in the theory section, the high frequency IMPS response (HF in Fig 7) should correspond to the ac component of the hole flux j_h into the surface, since the effects of surface recombination are effectively 'frozen out'. The HF plot therefore provides a direct measure of η_{coll}, which is given by j_h/qI_0. By contrast, the low frequency intercept (LF in Fig. 7) should correspond to the dc photocurrent (scaled by the 10% modulation depth), which is determined by the product $j_h(k_t/(k_t + k_r)$, where the ratio $k_t/(k_t + k_c)$ corresponds to η_{trans}, the fraction of hole flux from the space charge region that is involved in the charge transfer reaction. Fig. 9 shows how these two limiting currents (and hence η_{coll} and η_{trans}) vary with potential in the case of an untreated α-Fe_2O_3 electrode measured at low light intensity. It can be seen that the current corresponding to the HF limit increases with potential before appearing to saturate beyond 0.6 V vs. Ag|AgCl. The high frequency response corresponds to the hole current j_h, which rises as the width of the space charge region increases, enhancing the collection of holes from the interior of the oxide as predicted by the Gärtner equation (eq. 1). In principle, the width of the space charge region as a function of potential can be estimated from the HF response if the value of α is known.

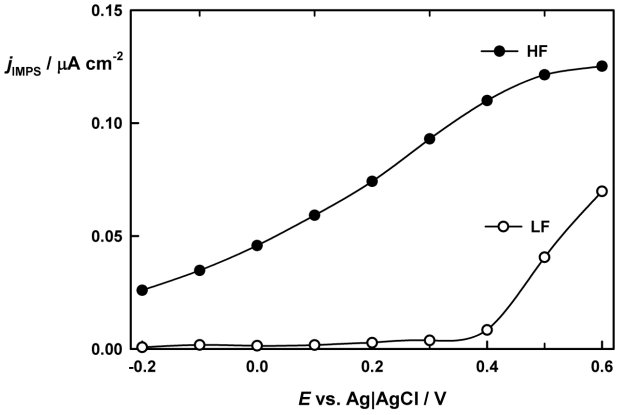

Fig. 9. Variation of the low frequency (LF) and high frequency (HF) limits of the IMPS response vary with potential. Untreated α-Fe_2O_3 electrode. Illumination 455 nm, dc photon flux 1.3 x 10^{15} cm^{-2}.

The onset potential of the high frequency photocurrent lies outside of the region where reliable analysis of the IMPS spectra is possible, but clearly it is considerably more negative than -0.2 V vs. Ag|AgCl. The low frequency photocurrent response, on the other hand, remains very low until the potential exceeds 0.4 V vs. Ag|AgCl. This indicates that surface recombination is dominant over an extraordinarily wide potential range for this sample. Even at the most positive potential, surface recombination still accounts for the loss of around 50% of the holes reaching the surface.

It is worth noting at this point that IPCE spectra are often recorded using chopped illumination. The slow response seen in the IMPS plot in Fig. 7, for example, indicates that very low chopping rates are required to obtain a true steady state photocurrent voltage plot. This is also clear from the photocurrent transients shown in Fig. 6.

Analysis of IMPS data obtained at different light intensities showed that the LF photocurrent voltage plots are displaced to more negative potentials as the light intensity is increased. This is illustrated by the normalized plots shown in Fig 10, where the photocurrents have been divided by the transmittance of the neutral density filters used to attenuate the illumination intensity.

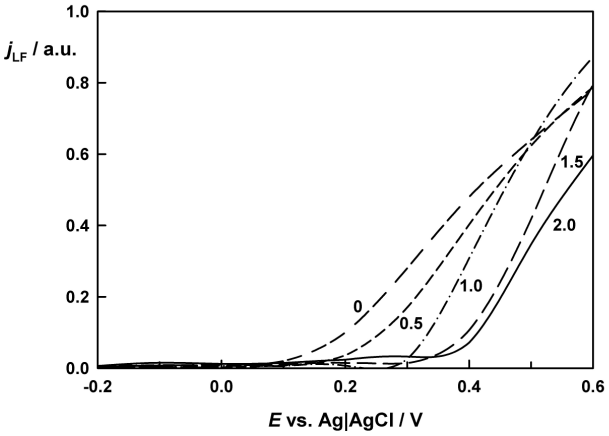

Fig. 10. Normalized plots of the low frequency photocurrent measured by IMPS for an untreated α-Fe_2O_3 electrode. The plots are labelled with the optical densities of the neutral density filters used. Note the negative displacement of the plots with increasing intensity.

The displacement, which is also observed in steady state photocurrent voltage curves (not shown), suggests that the ηtransfer = kt/(kt + kr) increases with light intensity. As shown below , this is confirmed from the complete analysis of the IMPS data.

Figure 11 is a semi-logarithmic plot showing the potential dependence of the kt and kr values derived from the IMPS response of an untreated α-Fe2O3 electrode at the highest light intensity (corresponding to OD 0 in Fig. 10). It is clear that both k_t and k_r depend on potential. The potential dependence of k_r is expected to be related to the surface concentration of electrons n_{surf} in the α-Fe_2O_3, which in turn depends on the bulk electron density n_{bulk} (determined by the doping density N_d) and on the band bending $\Delta\phi_{bb}$.

$$n_{surf} = n_{bulk} e^{-\frac{q\Delta\phi_{bb}}{k_B T}} \quad (3)$$

For an ideal semiconductor/electrolyte junction, the surface electron concentration should decrease by a factor of 10 for each 59 mV of additional reverse voltage bias. It is evident from Fig. 11 that this is not the case here. k_r varies by only two decades over the entire potential range, and in the centre of the plot, it remains almost constant. This behaviour is consistent with the presence of a high density of surface states that effectively 'metallize' the surface, causing Fermi level pinning. In this situation, changes in electrode potential predominantly affect the voltage drop in the Helmholtz layer, rather than in the semiconductor. Interestingly, the changes in Helmholtz potential drop appear to enhance the rate of charge transfer since k_r increases in the region where Fermi level pinning is most obvious. Again, this behaviour is consistent with 'metal-like' behaviour. It can be seen from Fig 11 that k_t only exceeds k_r when the potential becomes more positive than about 0.3 V vs. Ag|AgCl. This explains why the LF (or steady state) photocurrent onset potential is so positive.

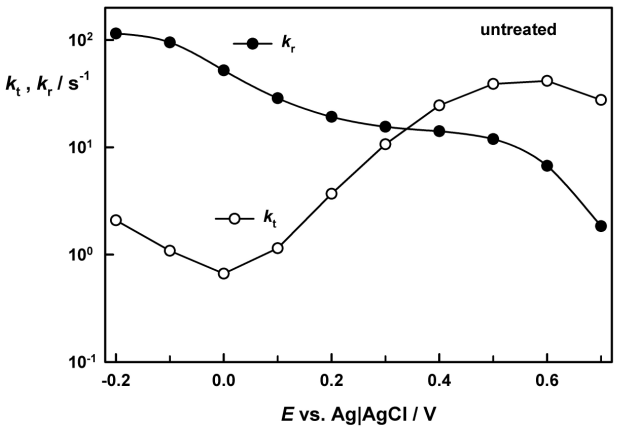

Fig. 11. Potential dependence of the rate constants k_t and k_r for an untreated α-Fe_2O_3 sample. Illumination 455 nm, dc photon flux 1.1 x 10^{17} cm^{-2} s^{-1}.

The trends in the values of k_t and k_r obtained from the analysis of the IMPS response are broadly similar to those derived previously from PEIS measurements.[14] However, the voltage range over which data can be derived is wider for IMPS.

The effects of treating the α-Fe_2O_3 electrodes with a cobalt(II) solution are remarkable. As Fig. 12 shows for the highest light intensity used, the LF and HF photocurrent plots corresponding to the intercepts in the IMPS response (cf. Fig. 7) move much closer together, indicating almost total suppression of surface recombination. This causes a large shift of the photocurrent onset towards more negative potentials, and the 'dc' photocurrent onset now occurs at -0.6 V vs. Ag|AgCl, which is close to reported values of the flat band potential for the α-Fe_2O_3.[8, 32, 33]

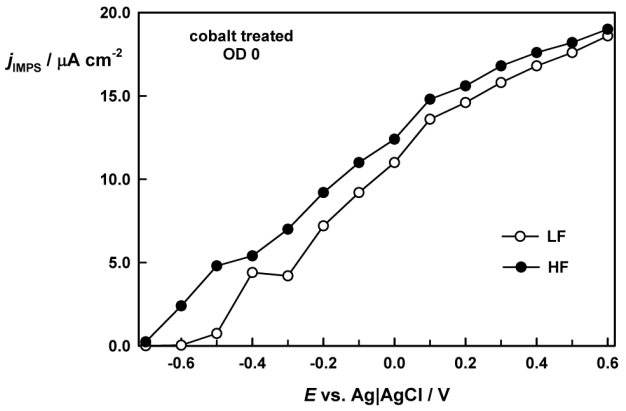

Fig. 12. HF and LF photocurrents for cobalt-treated α-Fe_2O_3 electrode. Illumination 455 nm, dc photon flux 1.1 x 10^{17} cm^{-2} s^{-1}.

The cobalt treatment also changes the potential dependence of k_t and k_r substantially. As Fig. 13 shows, k_t is now almost independent of electrode potential, whereas k_r decreases strongly with potential as expected for a more ideal semiconductor/electrolyte interface (cf. eq. 3). The most striking difference between Fig. 11 and Fig. 13 is the location of the crossover point where k_t is equal to k_r. The cobalt treatment shifts the crossover from around 0.3 V to ca. -0.5 V. Closer inspection of the two figures reveals that the displacement is predominantly due to strong suppression of surface recombination, and not to any increase in the rate constant for interfacial charge transfer. k_t is still remarkably small after the cobalt treatment, indicating that the effect of the treatment is not to catalyse the rate-determining step in oxygen evolution.

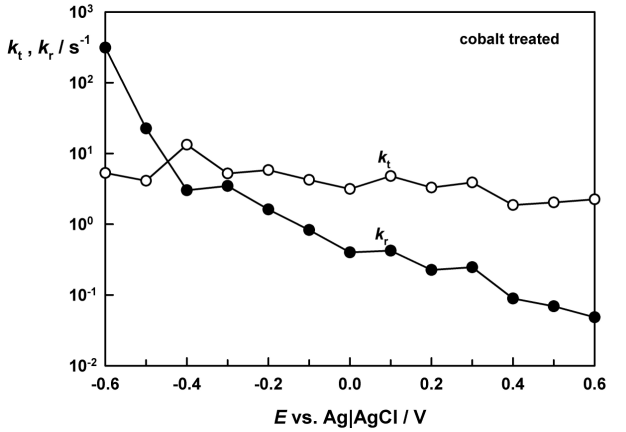

Fig. 13. Potential dependence of the rate constants k_r and k_r for a cobalt-treated α-Fe_2O_3 sample. Illumination 455 nm, dc photon flux 1.1 x 10^{17} cm^{-2} s^{-1}.

It is difficult to see how the cobalt treatment could affect the recombination pathways shown in Scheme III. It seems more likely that recombination occurs predominantly via surface states associated with other sites on the surface that are effectively 'passivated' by the adsorption of cobalt. Passivation of surface states by adsorption is well known for the case of semiconductors such as n-GaAs, where adsorption of ruthenium ions largely eliminates surface recombination. Nevertheless, it is surprising that recombination involving higher-valent Fe states appears not to play a major role. Since the rate constant for surface recombination depends on capture cross section for electrons, this may indicate that the higher-valent Fe states carry a negative charge due to surface OH^- groups.

Conclusions

The results of this study reveal that the charge transfer processes leading to oxygen evolution are very slow on α-Fe_2O_3, even after cobalt treatment. Contrary to expectations, the remarkable improvement of the current voltage characteristics brought about by the cobalt treatment is clearly due to the suppression of surface recombination rather than to catalysis of oxygen evolution. The study shows that IMPS should be a useful tool for assessing the effects of different types of surface modification of semiconductor electrodes, since it distinguishes between changes in the rates of surface recombination and charge transfer. Further work is in progress to identify the intermediates in the light-driven oxidation of water at α-Fe_2O_3 electrodes and to establish whether other surface modifications do indeed lead to enhancement of the rate of charge transfer, as is often claimed (largely without adequate experimental proof) in the literature.

Acknowledgments

KGUW and AAT acknowledge support from EPSRC.

Notes and references

[a] *Department of Chemistry, University of Bath, Bath BA2 7AY, United Kingdom. Tel: +44(0)1225 462883; e-Mail: l.m.peter@bath.ac.uk.*
[b] *Department of Chemistry, Loughborough University, Loughborough LE11 3TU, United Kingdom. Tel: +44(0)1509 22574; e-mail: u. wijayantha @lboro.ac.uk.*

1. M. Woodhouse and B. A. Parkinson, *Chem Soc Rev*, 2009, **38**, 197-210.
2. K. L. F. Sivula, F.; Gratzel, M., *ChemSusChem*, 2011, **4**, 432-449.
3. J. Brillet, M. Cornuz, F. Le Formal, J. H. Yum, M. Gratzel and K. Sivula, *Journal of Materials Research*, 2010, **25**, 17-24.
4. A. B. Murphy, P. R. F. Barnes, L. K. Randeniya, I. C. Plumb, I. E. Grey, M. D. Horne and J. A. Glasscock, *International Journal of Hydrogen Energy*, 2006, **31**, 1999-2017.
5. N. Iordanova, M. Dupuis and K. M. Rosso, *Journal of Chemical Physics*, 2005, **122**, 144305-144305-144310.
6. F. Le Formal, M. Gratzel and K. Sivula, *Advanced Functional Materials*, 2010, **20**, 1099-1107.
7. J. Brillet, M. Gratzel and K. Sivula, *Nano Letters*, 2010, **10**, 4155-4160.

8. A. A. Tahir, K. G. U. Wijayantha, S. Saremi-Yarahmadi, M. Mazhar and V. McKee, *Chemistry of Materials*, 2009, **21**, 3763-3772.
9. L. M. Peter and D. Vanmaekelbergh, in *Adv. Electrochem. Sci. Eng.*, Weinheim, 1999, vol. 6, pp. 77-163.
10. E. A. Ponomarev and L. M. Peter, *Journal of Electroanalytical Chemistry*, 1995, **396**, 219-226.
11. R. Peat and L. M. Peter, *Journal of Electroanalytical Chemistry*, 1987, **228**, 351-364.
12. E. A. Ponomarev and L. M. Peter, *J. Electroanal. Chem.*, 1995, **397**, 45-52.
13. D. J. Fermi, E. A. Ponomarev and L. M. Peter, *J. Electroanal. Chem.*, 1999, **473**, 192-203.
14. K. G. U. Wijayantha, S. Saremi-Yarahmadi and L. M. Peter, *Physical Chemistry Chemical Physics*, 2011, **13**, 5264-5270.
15. C. Y. Cummings, M. J. Bonne, K. J. Edler, M. Helton, A. McKee and F. Marken, *Electrochemistry Communications*, 2008, **10**, 1773-1776.
16. G. Larramona and C. Gutierrez, *Journal of the Electrochemical Society*, 1989, **136**, 2171-2178.
17. V. K. Sharma, F. Kazama, H. Jiangyong and A. K. Ray, *Journal of Water and Health*, 2005, **3**, 45-58.
18. H. Goff and R. K. Murmann, *Journal of the American Chemical Society*, 1971, **93**, 6058-&.
19. S. R. Pendlebury, M. Barroso, A. J. Cowan, K. Sivula, J. W. Tang, M. Gratzel, D. Klug and J. R. Durrant, *Chemical Communications*, 2011, **47**, 716-718.
20. A. Carrington, D. Schonland and M. C. R. Symons, *Journal of the Chemical Society*, 1957, 659-665.
21. V. K. Sharma, C. R. Burnett and F. J. Millero, *Physical Chemistry Chemical Physics*, 2001, **3**, 2059-2062.
22. K. Sivula, R. Zboril, F. Le Formal, R. Robert, A. Weidenkaff, J. Tucek, J. Frydrych and M. Gratzel, *Journal of the American Chemical Society*, 2011, **132**, 7436-7444.
23. K. J. McDonald and K.-S. Choi, *Chemistry of Materials*, 2011, **23**, 1686-1693.
24. M. W. Kanan and D. G. Nocera, *Science*, 2008, **321**, 1072-1075.
25. A. Kay, I. Cesar and M. Gratzel, *Journal of the American Chemical Society*, 2006, **128**, 15714-15721.
26. F. Le Formal, N. Tetreault, M. Cornuz, T. Moehl, M. Gratzel and K. Sivula, *Chemical Science*, 2011, **2**, 737-743.
27. R. Peat and L. M. Peter, *Journal of the Electrochemical Society*, 1986, **133**, C334.
28. L. M. Peter, E. A. Ponomarev and D. J. Fermin, *Journal of Electroanalytical Chemistry*, 1997, **427**, 79-96.
29. W. W. Gartner, *Physical Review*, 1959, **116**, 84.
30. S. Saremi-Yarahmadi, A. A. Tahir, B. Vaidhyanathan and K. G. U. Wijayantha, *Materials Letters*, 2009, **63**, 523-526.
31. J. C. Papaioannou, G. S. Patermarakis and H. S. Karayianni, *Journal of Physics and Chemistry of Solids*, 2005, **66**, 839-844.
32. J. H. Kennedy and K. W. Frese, *Journal of the Electrochemical Society*, 1978, **125**, 723-726.
33. S. U. M. Khan and J. Akikusa, *Journal of Physical Chemistry B*, 1999, **103**, 7184-7189.

